A Two-time-scale Model-based Combined Magnetic and Kinetic Control System for Advanced Tokamak Scenarios on DIII-D

Wenyu Shi, William Wehner, Justin Barton, Mark D. Boyer, Eugenio Schuster, Didier Moreau, Tim C. Luce, John R. Ferron, Michael L. Walker, David A. Humphreys, Ben G. Penaflor and Robert D. Johnson

***Abstract*— System identification techniques have been successfully used to obtain linear dynamic plasma response models around a particular equilibrium in different tokamaks. This paper identifies a two-time-scale dynamic model of the rotational transform ι profile and β_N in response to the electric field due to induction as well as to heating and current drive (H&CD) systems based on experimental data from DIII-D. The control goal is to regulate the plasma ι profile and β_N around a particular target value. A singular value decomposition (SVD) of the plasma model at steady state is carried out to decouple the system and identify the most relevant control channels. A mixed sensitivity H_∞ control design problem is solved to determine a stabilizing feedback controller that minimizes the reference tracking error and rejects external disturbances with minimal control energy. The feedback controller is augmented with an anti-windup compensator, which keeps the given controller well-behaved in the presence of magnitude constraints in the actuators and leaves the nominal closed-loop unmodified when no saturation is present. Experimental results illustrate the performance of the proposed controller, which is one of the first profile controllers integrating magnetic and kinetic variables ever implemented in DIII-D.**

I. Introduction

The tokamak, one of the most common devices for controlled nuclear fusion, is used to magnetically confine an ionized hydrogen gas, known as plasma, in a toroidal geometry in order to facilitate fusion reactions. The shape of the toroidal current density profile as a function of the tokamak's minor radius is critical for the development and sustainment of self-generated non-inductive current, which in turn serves as the enabler for steady-state operation. The current density profile is intimately related to the rotational transform ι profile, which is defined as the inverse of the safety factor q profile, which in turn is defined as the ratio of the number of times a magnetic field line goes toroidally around the tokamak to the number of times it goes around poloidally. The parameter β_N, defined as the normalized ratio between the internal kinetic pressure of the plasma and the external pressure of the magnetic field, is a key measure of performance used to gauge progress toward developing a power-producing fusion reactor. Therefore, real-time control of the ι profile and β_N is of paramount importance.

This work was supported by the National Science Foundation CAREER Award program (ECCS-0645086), and the U.S. Department of Energy (DE-FG02-09ER55064 and DE-FC02-04ER54698). W. Shi (wenyu.shi@lehigh.edu), W. Wehner, J. Barton, M.D. Boyer and E. Schuster are with the Department of Mechanical Engineering & Mechanics, Lehigh University, Bethlehem, PA 18015, USA. D. Moreau is with CEA, IRFM, 13108 Saint-Paul-lez-Durance, France. T.C. Luce, J.R. Ferron, M.L. Walker, D.A. Humphreys, B.G. Penaflor, and R.D. Johnson are with General Atomics, San Diego, CA 92121, USA.

As an alternative to first-principles modeling, system identification methods [1] have been successfully applied in different tokamaks. In the JET tokamak, a two-time-scale linear system has been used to describe the magnetic profiles around certain quasi-steady-state trajectories [2], [3]. By using input/output (I/O) diagnostic data, the current profile dynamic model has been identified for ASDEX Upgrade [4]. System identification experiments have been previously carried out on DIII-D [5] by the authors to develop identified models of the toroidal rotation profile [6] and the rotational transform profile [7].

This paper aims at designing a real-time ι profile and β_N integrated controller based on linear identified dynamic models from DIII-D. To cope with the slow dynamic of the magnetic parameter ι and the fast dynamic of the kinetic parameter β_N, the model identification procedure makes use of the timescale difference to produce a two-time-scale model. A singular value decomposition (SVD) [8] is used to decouple the system and identify the most relevant control channels at steady state. The mixed sensitivity H_∞ control method [9] is applied to synthesize a linear closed-loop controller. The feedback controller is then augmented with an anti-windup compensator [10], [11], which keeps the given controller well-behaved in the presence of actuator saturation. A profile control experiment integrating magnetic and kinetic variables for DIII-D in high-confinement mode (H-mode) illustrates the performance of the proposed controller.

This paper is organized as follows. In Section II, the system identification procedure for the DIII-D tokamak is briefly described, and an integrated two-time-scale dynamic model of the ι profile and β_N is developed. In Section III, the design of the plasma control algorithm is described. Computer simulation and experimental results from the DIII-D tokamak are presented in Section IV. Section V states the conclusions.

II. System Identification on DIII-D

System identification for the plasma rotational transform profile $\iota(\hat{\rho})$ is carried out with 5 Galerkin coefficients [2], [3], [6], [7] computed at $\hat{\rho} = 0.2, 0.4, 0.5, 0.6, 0.8$. The parameter $\hat{\rho}$ is defined as $\hat{\rho} = \frac{\rho}{\rho_b}$, where ρ is the mean geometric minor radius of the flux surface, i.e., $\pi B_{\phi,0}\rho^2 = \Phi$. The parameter Φ is the toroidal magnetic flux, and $B_{\phi,0}$ is the magnetic field at the geometric major radius. The parameter ρ_b is the mean geometric minor radius of the last closed magnetic flux surface.

To collect the data for system identification a number of discharges were run with identical ramp-up phases and different modulations of the various actuators around reference values during the flat-top phase [5]. The neutral beam injection (NBI), and electron cyclotron (EC) systems provided the heating and non-inductive current drive sources for these experiments. Available beam-lines and gyrotrons were grouped to form, together with I_p, five independent H&CD actuators: (*i*) plasma current I_p, (*ii*) co-current NBI power P_{CO}, (*iii*) counter-current NBI power P_{CT}, (*iv*) balanced NBI power P_{BL}, and (*v*) total EC power from all gyrotrons P_{EC}.

The relation between inputs and outputs is assumed as

$$y(t) = y_{FF} + \Delta y(t) = P_{FF}(u_{FF}) + P\Delta u(t), \tag{1}$$

where P_{FF} represents the relationship between the reference feedforward input u_{FF} and reference feedforward output y_{FF}. The variable $\Delta y(t)$ denotes the deviation output defined as $\Delta y(t) = [\Delta\iota(t),\ \Delta\beta_N(t)] = y(t) - y_{FF}$, with $y(t) = [\iota(0.2,t)\ \iota(0.4,t)\ \iota(0.5,t)\ \iota(0.6,t)\ \iota(0.8,t),\ \beta_N(t)]^T$. The variable Δu denotes the deviation input defined as $\Delta u = u - u_{FF}$ with $u = [I_p,\ P_{CO},\ P_{CT},\ P_{BL},\ P_{EC}]$. The linear model P is identified from experimental data using the prediction error method (PEM) according to a least squares fit criterion [1], and is expressed in state space form

$$\begin{aligned}\Delta\dot{\iota}(t) &= A_{11}\Delta\iota(t) + A_{12}\Delta\beta_N(t) + B_1\Delta u(t)\\ \varepsilon\Delta\dot{\beta}_N(t) &= A_{21}\Delta\iota(t) + A_{22}\Delta\beta_N(t) + B_2\Delta u(t),\end{aligned} \tag{2}$$

where the parameter ε represents the typical ratio between the energy confinement time and the characteristic resistive diffusion time. By defining an additional independent variable $\tau = t/\varepsilon$ to describe the fast dynamics while t describes the slow dynamics, the model can be expressed as a sum of a fast and a slow component depending on τ and t. Because there is no term of ε in the $\Delta\dot{\iota}(t)$ expansion, $\Delta\iota(t)$ has only a slow evolution. As in [5], the model can be expressed as a slow model,

$$\Delta\dot{\iota}(t) = A_s\Delta\iota(t) + B_s\Delta u_s(t) \qquad \Delta\beta_{Ns} = C_s\Delta\iota + D_s\Delta u_s, \tag{3}$$

and a fast model,

$$\Delta\dot{\beta}_{Nf}(t) = A_f\Delta\beta_{Nf}(t) + B_f\Delta u_f(t), \tag{4}$$

where $\Delta\beta_{Ns}$ and $\Delta\beta_{Nf}$ are the slow and fast parts of $\Delta\beta_N$, and Δu_s and Δu_f are the slow and fast parts of Δu.

In this work, we combine the slow model (3) and the fast model (4) with a first order low-pass filter to obtain the overall plant P. The lowest frequency at which the inputs could be filtered while retaining a good fit of the unfiltered ι data by the slow model in DIII-D was found to be around 1 Hz [5]. The filter is written as

$$\begin{aligned}\dot{X}_{filter} &= -2\pi X_{filter} + 2\pi\Delta u\\ \begin{bmatrix}\Delta u_s\\ \Delta u_f\end{bmatrix} &= \begin{bmatrix} I\\ -I\end{bmatrix} X_{filter} + \begin{bmatrix}0\\ I\end{bmatrix}\Delta u,\end{aligned} \tag{5}$$

where X_{filter} is the state, and I is the identity matrix. Substituted (5) into (3) and (4), the ι and β_N combined model can be obtained as

$$\begin{aligned}\begin{bmatrix}\Delta\dot{\iota}\\ \Delta\dot{\beta}_{Nf}\\ \dot{X}_{filter}\end{bmatrix} &= \begin{bmatrix}A_s & 0 & B_s\\ 0 & A_f & -B_f\\ 0 & 0 & -2\pi\end{bmatrix}\begin{bmatrix}\Delta\iota\\ \Delta\beta_{Nf}\\ X_{filter}\end{bmatrix} + \begin{bmatrix}0\\ B_f\\ 2\pi\end{bmatrix}\Delta u\\ &= A\begin{bmatrix}\Delta\iota\\ \Delta\beta_{Nf}\\ X_{filter}\end{bmatrix} + B\Delta u\\ \begin{bmatrix}\Delta\iota\\ \Delta\beta_N\end{bmatrix} &= \begin{bmatrix}I & 0 & 0\\ C_s & I & D_s\end{bmatrix}\begin{bmatrix}\Delta\iota\\ \Delta\beta_{Nf}\\ X_{filter}\end{bmatrix} = C\begin{bmatrix}\Delta\iota\\ \Delta\beta_{Nf}\\ X_{filter}\end{bmatrix}.\end{aligned} \tag{6}$$

More details on the system identification procedure can be obtained from our previous work [6], [7].

III. Control System Design

A MIMO H_∞ controller based on the overall dynamic model (6) is described in this section. The control algorithm is summarized by the following steps: (1) decouple the system at steady state and identify the most relevant control channels (Section III-A), (2) design an H_∞ controller $\hat{K}$ ignoring control input saturation (Section III-B), (3) add the anti-windup compensator *AW* to minimize the adverse effect of any control input saturation (Section III-C).

A. Singular Value Decomposition

The relation between the inputs and the outputs in the linear dynamic model (6) can be expressed in terms of its transfer function $P(s)$, i.e.,

$$\frac{\Delta Y(s)}{\Delta U(s)} = P(s) = C(sI - A)^{-1}B \tag{7}$$

where s denotes the Laplace variable and $\Delta Y(s)$ and $\Delta U(s)$ denote the Laplace transforms of the output Δy and the input Δu respectively. Assuming a constant target $\Delta\bar{y}_{tar}$ and closed-loop stabilization, the system will reach steady state as $t \to \infty$. It is possible to define $\Delta\bar{y} = \lim_{t\to\infty}\Delta y(t)$, $\Delta\bar{u} = \lim_{t\to\infty}\Delta u(t)$, and $\bar{e} = \lim_{t\to\infty} e(t) = \Delta\bar{y}_{tar} - \Delta\bar{y}$. Therefore, under these assumptions the closed-loop system is specified by

$$\Delta\bar{y} = \bar{P}\Delta\bar{u} = -CA^{-1}B\Delta\bar{u} \quad \Delta\bar{u} = \bar{\hat{K}}\bar{e} = \bar{\hat{K}}\left(\Delta\bar{y}_{tar} - \Delta\bar{y}\right), \tag{8}$$

where $\hat{K}(s)$ represents the transfer function of the to-be-designed controller and $\bar{\hat{K}} = \hat{K}(0)$.

In order to weight the control effort and tracking error, two positive definite weighting matrices $R \in \Re^{m\times m}$ and $Q \in \Re^{p\times p}$ are introduced to the system, where $p = 6$ is the number of outputs and $m = 5$ is the number of inputs. We then define the "weighted" steady-state transfer function, and its singular value decomposition (SVD) as $\tilde{P} = Q^{1/2}\bar{P}R^{-1/2} = USV^T$, where $S = \mathrm{diag}(\sigma_1, \sigma_2, \cdots, \sigma_m) \in \Re^{m\times m}$, $U \in \Re^{p\times m}$ ($U^TU = I$), and $V \in \Re^{m\times m}$ ($V^TV = VV^T = I$). The steady-state input-output relation is expressed as $\Delta\bar{y} = Q^{-1/2}\tilde{P}R^{1/2}\Delta\bar{u} = Q^{-1/2}USV^TR^{1/2}\Delta\bar{u}$. By invoking the properties of the SVD, the matrix $Q^{-1/2}US$ defines a basis of the steady-state output values, and the matrix $R^{-1/2}V$ defines a basis of the steady-state input values. A square decoupled system is obtained, and a one-to-one relationship between the inputs and outputs of the decoupled system is expressed as

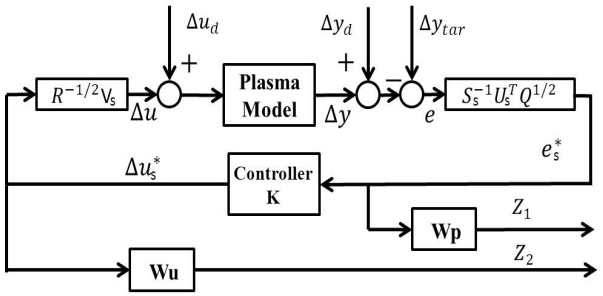

Fig. 1. H_∞ control formulation.

$$\Delta\bar{y}^* = S^{-1}U^TQ^{1/2}\Delta\bar{y} = S^{-1}U^TQ^{1/2}Q^{-1/2}USV^TR^{1/2}\Delta\bar{u} = \Delta\bar{u}^*,$$

where $\Delta\bar{y}^* = S^{-1}U^TQ^{1/2}\Delta\bar{y}$ and $\Delta\bar{u}^* = V^TR^{1/2}\Delta\bar{u}$. By defining $\Delta\bar{y}^*_{tar} = S^{-1}U^TQ^{1/2}\Delta\bar{y}_{tar}$, the steady state tracking error is written as

$$\bar{e} = \lim_{t\to\infty} e(t) = \Delta\bar{y}_{tar} - \Delta\bar{y} = Q^{-1/2}US(\Delta\bar{y}^*_{tar} - \Delta\bar{y}^*). \quad (9)$$

Substituting this expression into performance index, we can obtain the steady state cost function $\bar{J}$:

$$\bar{J} = (\Delta\bar{y}^*_{tar} - \Delta\bar{y}^*)^TS^2(\Delta\bar{y}^*_{tar} - \Delta\bar{y}^*) = \sum_{i=1}^{m}\sigma_i^2(\Delta\bar{y}^*_{tar_i} - \Delta\bar{y}^*_i)^2.$$

It is usually the case where $\sigma_1 > \cdots \sigma_k \gg \sigma_{k+1} > \cdots > \sigma_m > 0$. Therefore, it is possible that with the intent of minimizing $\bar{J}$ we will spend a lot of control effort to minimize the i^{th} component of the tracking error, for $i > k$, which has a very small contribution to the overall value of the cost function. To avoid spending a lot of control effort for a marginal improvement of the cost function value, we partition the singular value set into significant singular values S_s and negligible singular values S_n [8]. We can write $U = \begin{bmatrix} U_s & U_n \end{bmatrix}$, $V = \begin{bmatrix} V_s & V_n \end{bmatrix}$, $S = \text{diag}(S_s,\ S_n) \approx \text{diag}(S_s,\ 0)$, and approximate the cost function $\bar{J}$ by

$$\bar{J}_s = \sum_{i=1}^{k}\sigma_i^2(\Delta\bar{y}^*_{tar_i} - \Delta\bar{y}^*_i)^2 = (\Delta\bar{y}^*_{tar_s} - \Delta\bar{y}^*_s)^TS_s^2(\Delta\bar{y}^*_{tar_s} - \Delta\bar{y}^*_s),$$

where $\Delta\bar{y}^*_{tar_s} = S_s^{-1}U_s^TQ^{1/2}\Delta\bar{y}_{tar}$, $\Delta\bar{y}^*_s = S_s^{-1}U_s^TQ^{1/2}\Delta\bar{y}$, $\bar{e}^*_s = \Delta\bar{y}^*_{tar_s} - \Delta\bar{y}^*_s$ and $\Delta\bar{u}^*_s = V_s^TR^{1/2}\Delta\bar{u}$. The matrix basis reduce to $Q^{-1/2}U_sS_s$ and $R^{-1/2}V_s$, and the decoupled system,

$$P_{DC} = S_s^{-1}U_s^TQ^{1/2}PR^{-1/2}V_s, \quad (10)$$

represents a one-to-one relationship between the inputs $\Delta\bar{u}^*_s$ and the outputs $\Delta\bar{y}^*_s$.

B. Design of the Mixed Sensitivity H_∞ Controller

The mixed sensitivity H_∞ method is used to design the plasma controller. The design is based on the decoupled plasma model (10) and ignores control input saturation. The structure of the proposed controller is shown in Fig. 1, where two frequency-dependent weighting functions, W_p and W_u, are introduced for the tracking error and the input effort. The signals of the general control configuration are defined as the control input is Δu^*_s, the tracking error e^*_s, the exogenous reference is $\Delta y^*_{tar_s}$, and the external performance signal is $[Z_1,\ Z_2]^T = [W_pe^*_s,\ W_u\Delta u^*_s]^T$.

The feedback system shown in Fig. 1, now expressed in the conventional $P^* - K$ robust control framework, is shown in Fig. 2, where P^* is the generalized plant and

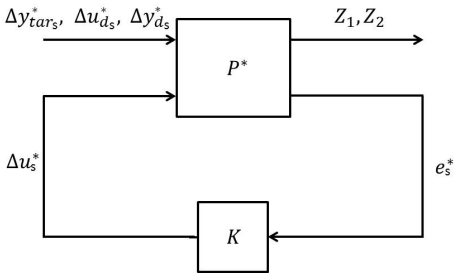

Fig. 2. Model in $P^* - K$ control framework.

K is the feedback controller. Using the Laplace Transform we can obtain a frequency-domain representation of the overall system. The plant $P^*(s)$ is the transfer function from the input signals $[\Delta y^{*T}_{tar_s},\ \Delta u^{*T}_{d_s},\ \Delta y^{*T}_{d_s},\ \Delta u_s{}^{*T},]^T$ to the output signals $[Z_1^T,\ Z_2^T,\ e_s^{*T}]^T$ and expressed as

$$\left[\begin{array}{c} Z_1 \\ Z_2 \\ \hline e^*_s \end{array}\right] = P^*(s)\left[\begin{array}{c} \Delta y^*_{tar_s} \\ \Delta u^*_{d_s} \\ \Delta y^*_{d_s} \\ \hline \Delta u^*_s \end{array}\right] = \left[\begin{array}{c|c} \tilde{P}_{11}(s) & \tilde{P}_{12}(s) \\ \hline \tilde{P}_{21}(s) & \tilde{P}_{22}(s) \end{array}\right]\left[\begin{array}{c} \Delta y^*_{tar_s} \\ \Delta u^*_{d_s} \\ \Delta y^*_{d_s} \\ \hline \Delta u^*_s \end{array}\right]$$

$$\tilde{u} = K(s)\tilde{e}. \quad (11)$$

The closed-loop transfer function from input signals $w = [\Delta y^{*T}_{tar_s},\ \Delta u^{*T}_{d_s},\ \Delta y^{*T}_{d_s}]^T$ to output signals $z = [Z_1,\ Z_2]$ is given by the lower linear fractional transformation (LFT), i.e.,

$$T_{zw} = F_l(P^*, K) = \tilde{P}_{11} + \tilde{P}_{12}K(I - \tilde{P}_{22}K)^{-1}\tilde{P}_{21}. \quad (12)$$

We define the sensitivity function $M_s = (I + P_{DC}K)^{-1}$, and write the closed-loop transfer function as

$$T_{zw} = F_l(P^*, K) = \begin{bmatrix} W_pM_s & -W_pM_sP_{DC} & -W_pM_s \\ W_uKM_s & -W_uKM_s & -W_uKM_s \end{bmatrix}.$$

We seek a controller $K(s)$ that stabilizes the system and minimizes the H_∞ norm of the transfer function $T_{zw}(P^*, K)$,

$$\min_{K(s)} \|T_{zw}(P^*, K)\|_\infty = \min_{K(s)}(\sup_\omega \bar{\sigma}[T_{zw}(P^*, K)(j\omega)]) \quad (13)$$

where $\bar{\sigma}$ represents the maximum singular value. This statement defines a mixed sensitivity H_∞ control problem, where the goal is to minimize the tracking error while using as little feedback control effort as possible. The frequency response of the magnitude of the maximum singular value of the upper bounds $1/W_p$ and $1/W_u$ along with the achieved transfer functions M_s, KM_s, and M_sP_{DC} computed with the feedback controller K are shown in Fig. 3. As can be seen from Fig. 3 (a-b), the frequency responses of the magnitudes of the closed-loop transfer functions are very close to their respective upper bounds, and the tracking goal of the closed-loop system with minimum control energy is therefore achieved. From Fig. 3 (c), we find that the controller can successfully reject input disturbances at low frequencies but it cannot reject input disturbances at some higher frequencies.

The input applied to the original system P is Δu, and the measurement available from the P is the error signal e. Therefore, we must convert the input and output of the controller to these signals. This is accomplished with the relationships $e^*_s = S_s^{-1}U_s^TQ^{1/2}e$ and $\Delta u = R^{-1/2}V_s\Delta u^*_s$.

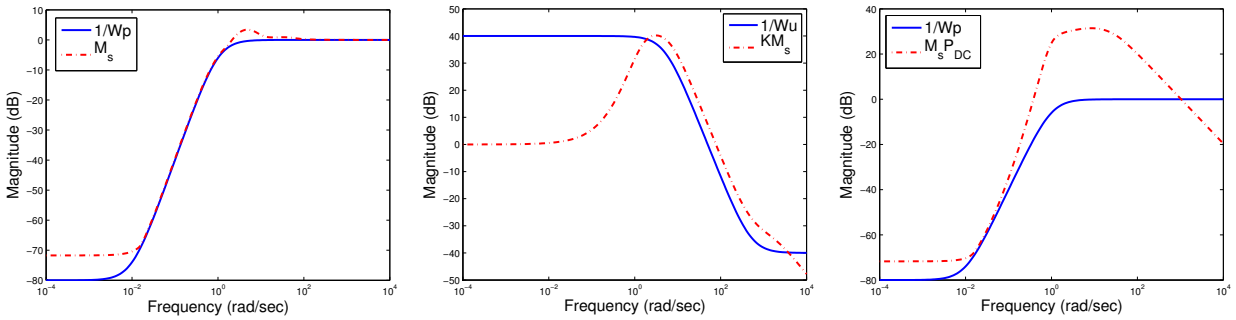

(a) (b) (c)

Fig. 3. Maximum singular value diagram of: (a) inverse of performance weight $1/W_p$ and sensitivity function M_s, (b) inverse of performance weight $1/W_u$ and control sensitivity function KM_s, and (c) inverse of performance weight $1/W_p$ and process sensitivity function M_sP_{DC}.

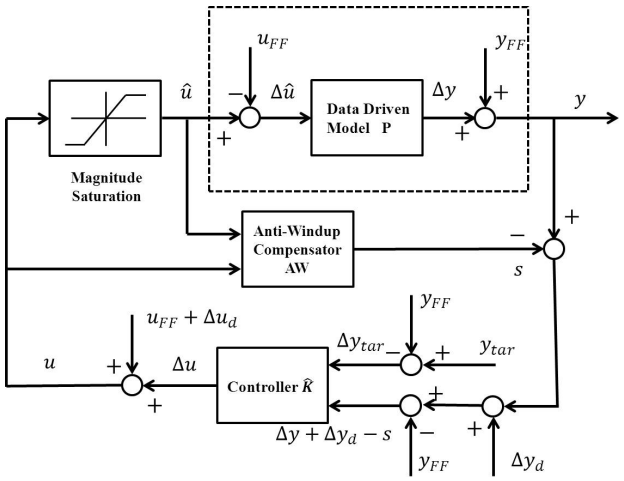

Fig. 4. DIII-D ι-profile control system architecture.

Finally, the overall plasma rotational transform ι profile and β_N controller for system P can be written as

$$\hat{K}(s) = \frac{\Delta U(s)}{E(s)} = R^{-1/2} V_s K(s) S_s^{-1} U_s^T Q^{1/2} \qquad (14)$$

where $\Delta U(s)$ denotes the Laplace transform of $\Delta u(t)$, and $E(s)$ denotes the Laplace transform of $e(t)$.

C. Design of the Anti-windup Compensator

The input saturation of each channel in DIII-D is shown in Table I. At the moment of designing the H_∞ controller, the actuator saturations were not considered. As a result of saturation, the actual plant input may be different from the output of the controller. When this happens, the controller output does not drive the plant and as a result, the states of the controller are wrongly updated, which can cause the behavior of the system to deteriorate dramatically, or even become unstable. The goal is to design an anti-windup compensator that works with the H_∞ controller to keep it well-behaved and avoid undesirable oscillations when saturation is present. The anti-windup augmentation is written as

$$\begin{aligned} \dot{x}_{aw} &= A_{aw}x_{aw} + B_{aw}(\hat{u} - u) + \gamma(u,\hat{u})\lambda \\ s &= C_{aw}x_{aw} + D_{aw}(\hat{u} - u) \\ \lambda &= -cx_{aw} - A_{aw}x_{aw} - B_{aw}(\hat{u} - u) \end{aligned} \qquad (15)$$

TABLE I

ACTUATOR LIMITS IN DIII-D

Channel	Actuator	Min	Max	Units
1	Ip	0.3	1.5	MA
2	Co-beam Power	0	12.5	MW
3	Ct-beam Power	0	5	MW
4	Balanced-beam Power	0	2.5	MW
5	Total EC Power	0.3	3	MW

TABLE II

THE VALUES OF INPUT DISTURBANCES

ΔI_{p_d}	ΔP_{CO_d}	ΔP_{CT_d}	ΔP_{BL_d}	ΔP_{EC_d}
0.1 MA	0.1 MW	0 MW	-0.1 MW	0MW

where c is a positive constant, $\gamma(u,\hat{u}) = 1$ if $u = \hat{u}$ and 0 otherwise. The saturation function $\hat{u}$ is defined as

$$\hat{u} = sat_{u_{min}}^{u_{max}}(u) = \begin{cases} u_{max} & \text{if } u_{max} < u \\ u & \text{if } u_{min} < u < u_{max} \\ u_{min} & \text{if } u < u_{min} \end{cases}, \qquad (16)$$

where u_{max} and u_{min} is the maximum and minimum saturation limit. In our case, we decided to choose A_{aw}, B_{aw}, C_{aw}, and D_{aw} equal to the matrices of the plant P in (6) [10], [11].

The whole control system including the MIMO H_∞ controller and the anti-windup compensator is shown in Fig. 4. The proposed feedforward + feedback control scheme has been tested in simulations and experiments.

IV. SIMULATION AND EXPERIMENT RESULTS

In order to obtain relevant simulation results, we choose the same feedforward control inputs and input disturbances in both experiment and simulation. The reference feedforward inputs are $I_p = 0.9$ MA, $P_{CO} = 1.9838$ MW, $P_{CT} = 0$ MW, $P_{BL} = 2$ MW, and $P_{EC} = 1.4415$ MW. The input disturbances $\Delta u_d = [\Delta I_{p_d}, \Delta P_{CO_d}, \Delta P_{CT_d}, \Delta P_{BL_d}, \Delta P_{EC_d}]^T$, shown in Table II, are applied at $t = 3$ s. The feedback control component Δu is turned on and off throughout the discharge as

$$\Delta u = \begin{cases} \text{OFF} & \text{0 to 2.5 second} \\ \text{ON} & \text{2.5 to 4.75 second} \\ \text{OFF} & \text{4.75 to 5 second} \\ \text{ON} & \text{5 to 6 second} \end{cases}. \qquad (17)$$

Due to the large difference between plasma resistivity at the center and at the edge, the current density rapidly equilibrates at the edge, and evolves slowly in the center. Because it is difficult to control the ι values in the center of the plasma, it is possible that we spend a lot of control

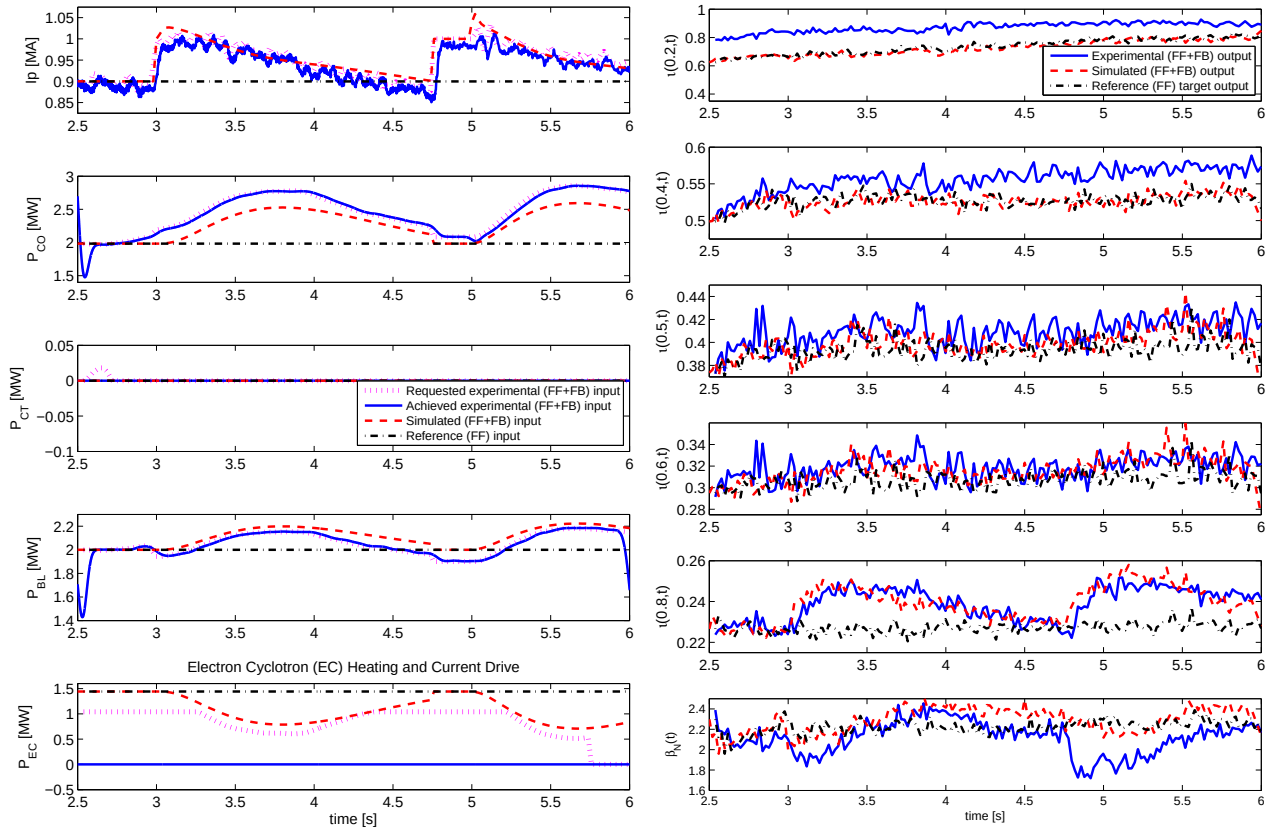

Fig. 5. DIII-D shot 147707: ι profile and β_N control – (a) Reference (FF), simulated (FF+FB), requested experimental (FF+FB) and achieved experimental (FF+FB) inputs, (b) Experimental (FF+FB), simulated (FF+FB) and reference (FF) ι target profile at $\hat{\rho} = 0.2, 0.4, 0.5, 0.6, 0.8$ and β_N.

effort to minimize the tracking error at $\iota(0.2,t)$ without any significant improvement in overall performance. Therefore, we take $Q = \text{diag}([0.05,\ 0.1,\ 1,\ 1,\ 1,\ 1])$ to reduce the weights of the tracking errors of $\iota(0.2,t)$ and $\iota(0.4,t)$. The plasma current I_p plays the most significant role in the ι profile, and the counter-current beam was not available in the experiment; therefore, the matrix is set as $R = \text{diag}([0.1,\ 0.25,\ 1000,\ 0.5,\ 0.25])$. The parameter c in (15) is set as 0.1 to make x_{aw} converge to zero arbitrarily fast ($\dot{x}_{aw} = -cx_{aw}$), and therefore to reset the state of the anti-windup compensator, when no actuator saturation is present. The experimental time interval is $[t_i,\ t_f] = [2.5,\ 6]$, and this same time interval is chosen for the simulation study. In order to compare simulation and experimental results, we plot them in the same pictures (Fig. 5).

A. Closed-loop Simulation

In the first 0.5 second of the simulation, the controller effectively regulates ι and β_N around the target values, afterwards the controller tries to reject the input disturbance. The simulated results (red dashed lines) with disturbance are shown in Fig. 5. The simulated plasma current I_p is shown in Fig. 5 (a.1), and the beam and total gyrotron powers are shown in Fig. 5 (a.2)-(a.5). The input disturbance is rejected quickly, and the plasma current, beams and gyrotron are not saturated during the simulation. The simulated outputs (red dashed lines) are shown in Fig. 5 (b). In the first 0.5 second, the regulation results are very good for all control points. When the disturbance is switched on at $t = 3$ s, $\iota(0.6,t)$, $\iota(0.8,t)$ ramp up and β_N decreases. Due to the weight matrix Q, control effort is mainly applied to the edge value of the ι profile and β_N. The controller rejects the effects of the input disturbance and fixes the errors quickly. The ι values at $\hat{\rho} = 0.5, 0.6, 0.8$ and β_N come back to the target values at around $t = 4.5$ s. When the controller is turned off at $t = 4.75$ s, the ι values and β_N drift away from the target values again. In the last second, the feedback controller is turned on again and the tracking errors become much smaller.

B. Closed-loop Experiments on DIII-D

Shot # 147707 was used to test the combined controller for ι profile and β_N. Fig. 5 (a) shows the feedforward (black dotted line), requested feedforward+feedback (dotted-dashed line) and achieved feedforward+feedback (solid blue lines) physical actuations during the experiment. The plasma current (Fig. 5 (a.1)) and the beams (Fig. 5 (a.2)-(a.4)) successfully followed the requested values without exhibiting any saturation. The EC, used for plasma heating, was off during the experiment. This, combined with the lack of counter-injection beams, made the control of the inner ι profile very difficult. It can be noted from Fig. 6 (a) that it was indeed not possible to reproduce the target profile in

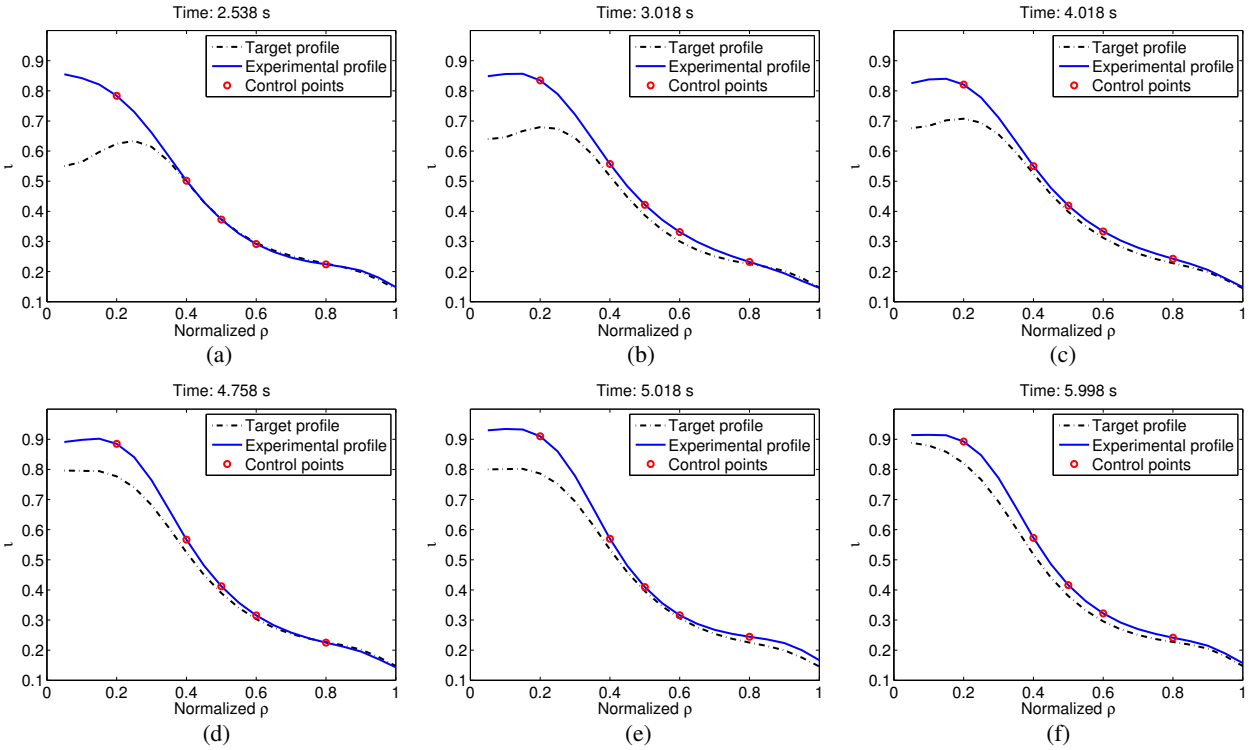

Fig. 6. Experimental $\iota(\hat{\rho})$ profile at time t= 2.538, 3.018, 4.018, 4.758, 5.018, 5.998 seconds from DIII-D shot # 147707.

the center of the plasma ($\iota(0.2,t)$) at the beginning of the closed-loop control experiment ($t = 2.5$ s). The difference between achieved and requested values of P_{EC} (Fig. 5 (a.5)) can be interpreted as an additional disturbance to be rejected by the controller. The experimental outputs (solid blue lines) are shown in Fig. 5 (b). Note that both the ι profile and β_N recovered their target values after the transient produced by the injection of disturbances at $t = 3$ s. When the controller was turned off at $t = 4.75$ s, the actuator values drifted away from the feedforward values immediately and a tracking error became noticeable particularly for β_N and the outer ι profile. Finally, the feedback controller was turned on at $t = 5$ s and drove back the ι profile and β_N to their target values, rejecting once again the effects of the input disturbance. A series of six plasma profiles at different times are shown in Fig. 6. After the input disturbances were applied to the tokamak, these tracking errors became larger, as shown in Fig. 6 (b). As time went on in shot # 147707, the tracking errors became smaller as shown in Fig. 6 (c), (d) thanks to the action of the feedback controller. When the feedback controller was turned off, the tracking errors increased once again as shown in Fig. 6 (e) before finally recovered after the controller was turned back on as shown in Fig. 6 (f).

V. Conclusion

An H_∞, model-based, MIMO, ι-profile and β_N controller has been designed for the DIII-D tokamak. The design is based on a two-time-scale linear dynamic plasma response model around a reference profile during the current flat-top phase. The feedback controller can regulate the system around the target, which is close to the reference equilibrium, even in the presence of various disturbances. The proposed controller, which has been tested experimentally in H-mode on DIII-D, represents one of the first profile controllers integrating magnetic and kinetic variables ever implemented in DIII-D. Because of the lack of counter beam and EC power, the inner ι was not well controlled. The improvement of inner ι profile control is part of our future work.

References

[1] L. Ljung, *System Identification: Theory for the User*. Prentice Hall PTR, 1999.

[2] D. Moreau, *et al.*, "Real-time Control of the q-profile in JET for Steady State Advanced Tokamak Operation," *Nuclear Fusion*, vol. 43, pp. 870–882, 2003.

[3] ——, "A Two Time Scale Dynamic Model Approach for Magnetic and Kinetic Profile Control in Advanced Tokamak Scenarios on JET," *Nuclear Fusion*, vol. 48, pp. 1–38, 2008.

[4] Y. S. Na, "Modeling of Current Profile Control in Tokamak Plasmas," Ph.D. dissertation, Fakultat fur Physik: Technische Universitat Munchen, Munich, Germany, 2003.

[5] D. Moreau, *et al.*, "Plasma Models for Real-time Control of Advanced Tokamak Scenarios," *Nuclear Fusion*, vol. 51, pp. 1–14, 2011.

[6] W. Wehner *et al.*, "Data-driven Modeling and Feedback Tracking Control of the Toroidal Rotation Profile for Advanced Tokamak Scenarios in DIII-D," in *Proceeding of the 2011 IEEE Multiconference on Systems and Control*, 2011.

[7] W. Shi *et al.*, "Multivariable Robust Control of the Plasma Rotational Transform Profile for Advanced Tokamak Scenarios in DIII-D," in *Proceeding of 2012 American Control Conference*, 2012.

[8] G. Ambrosino *et al.*, "Optimal Steady-state Control for Linear Non-right-invertible systems," *IET Control Theory & Applications*, vol. 1, no. 3, pp. 604–610, 2007.

[9] S. Skogested and I. Postlethwaite, *Multivariable Feedback Control*. John Wiley and Sons, Ltd, 2003.

[10] E. Schuster *et al.*, "Antiwindup Scheme for Plasma Shape Control with Rate and Magnitude Actuation Constraints in the DIII-D Tokamak," in *Proceeding of the 2003 IEEE International Conference on Decision and Control*, 2003.

[11] A. R. Teel, "Dynamic Anti-windup for Nonlinear Control Systems," *IEEE Transaction of Automatic Control*, 2004.